Optimization of CO_2 Capture Process Using Dry Sodium-Based Sorbents

Kazemi, Hossein; Shahhosseini, Shahrokh*[+]; Amiri, Mohsen

School of Chemical, Petroleum and Gas Engineering, Iran University of Science and Technology
Tehran, I.R. IRAN

ABSTRACT: *Sodium carbonate (Na_2CO_3) supported by gamma-alumina (γ-Al_2O_3) is one of the best sorbents for CO_2 capture in economic terms because of its low raw material cost and excellent performance in low-temperature operation. The fundamental goal of this study is to optimize the operating conditions of CO_2 adsorption by Na_2CO_3/Al_2O_3 sorbent in a fixed bed reactor. The sorbent characterization was studied using BET, SEM, XRF, and XRD analyses, and the sorbent structure was compared before and after the carbonation reaction. Moreover, the effects of side reactions on the adsorption process were investigated. The Response Surface Methodology (RSM) was used with Box-Behnken Design (BBD) to design the experiments. The optimum conditions are introduced at the point where initial CO_2 capture capacity and deactivation rate constants are as high and as low as possible, respectively. The optimum values of the variables corresponding to the temperature of 50°C, vapor pretreatment time of 9 min, and H_2O/CO_2 mole ratio of 1. The amounts of initial CO_2 capture capacity and deactivation rate constant in the optimum conditions were obtained to be 39.238 $mgCO_2/g_{sorbent}$ and 0.416 min^{-1}, respectively.*

KEYWORDS: *CO_2 capture; Alkali metal carbonate; Operating parameter optimization; Response Surface Methodology (RSM); Carbonation reaction; Carbonation kinetics.*

INTRODUCTION

The presence of greenhouse gases in the atmosphere is the main reason for global warming [1]. Greenhouse gases mainly consist of carbon dioxide (CO_2), methane (CH_4), halocarbon gases ($CFCl_3$ and CF_2Cl_2), nitrogen oxide (N_2O), and sulfur hexafluoride (SF_6) [2]. It has been reported that the average global temperature is raised by 0.74% over the last 100 years [2]. CO_2 has the highest percentage of greenhouse gases, and about 24 billion tons of CO_2 is annually produced [3,4]. Fossil fuel combustion in power plants is the primary source of anthropogenic CO_2 emission [5,6]. In addition to climate changes, the emission of CO_2 can contribute to health problems, acid rain, and urban smog [7,8].

Different materials and technologies have been applied to control the combustion process to reduce CO_2 emissions [9]. Combustion-related CO_2 capture technologies can be organized as pre-combustion, oxy-fuel combustion, and post-combustion [2]. The pre-combustion technology is widely used in hydrogen and fertilizer production. Economic exploitation of this method requires long-term

* *To whom correspondence should be addressed.*
+ *E-mail: shahrokh@iust.ac.ir*
1021-9986/2021/4/1179-1194 *16/$/6.06*

developments in the fields of hydrogen turbine, gasification, syngas cleaning, gas separation, and fuel cells [10]. In the oxy-fuel process, since high-purity oxygen is used instead of air for combustion, the reaction products mainly consist of H_2 and CO_2 facilitating the separation process. However, providing high-purity O_2 for this process requires a lot of energy [2].

The post-combustion method is classified into three general categories: adsorption, absorption, and membrane separation [10]. A liquid amine-based absorption process has been used for CO_2 capture in recent years. This process has some problems such as poisoning from SO_x, NO_x, and O_2, low thermal stability, and high capital & operating costs [11,12]. A membrane-based process has some advantages such as low energy consumption and smooth operation. However, it is inappropriate for capturing massive volumes of CO_2 and requires a high-cost module [2]. Therefore, adsorption technology has been developed to control CO_2 emissions due to lower cost, simplicity of operation, and applicability in a wide range of temperature and pressure conditions [13,14]. Among common CO_2 adsorbents, alkali-metal-based solid sorbents attract considerable attention due to their lower energy requirements and excellent efficiency [10,15,16]. According to the below reaction, alkali metal carbonate react with CO_2 and H_2O at a low temperature (50-80°C) and transforms to alkali metal hydrogen carbonate [17].

$$M_2CO_3 + CO_2 + H_2O \Leftrightarrow 2MHCO_3$$

The enthalpies of this reaction for Na and K are -132.59 and -141.17 kJ/mol, respectively [18]. Regeneration reaction occurs at a temperature lower than 300 ºC [6,19]. K_2CO_3-based sorbent has been studied more than Na_2CO_3-based sorbent due to its higher adsorption capacity and reaction rate. However, using Na_2CO_3 in comparison with K_2CO_3 has some advantages such as higher availability and lower price and operating cost [20–23]. When Na_2CO_3 is used, R1 can be written as follows:

$$Na_2CO_3 + CO_2 + H_2O \Leftrightarrow 2NaHCO_3$$

In order to improve the sorbent performance, a porous matrix is usually used as support [24–27]. Several researchers have applied this sorbent on various supports, such as active carbon, zeolites, Al_2O_3, MgO, TiO_2, FeOOH, $TiO(OH)_2$, ZrO_2, and SnO_2 [23,28–34]. Between these supports, γ-Al_2O_3 is widely utilized as support in heterogeneous catalysis due to its thermal stability, high porosity, and high mechanical strength [20,35–37].

According to the literature, when Na_2CO_3 and K_2CO_3-based sorbents are applied, the most influential factors affecting the adsorption capacity are temperature, CO_2 concentration, H_2O concentration, and vapor pretreatment time [38–45]. The CO_2 adsorption mechanism through different reactions and the effect of operating conditions on the reaction conversion has also been investigated for Na_2CO_3 and K_2CO_3-based sorbents [46–49]. An essential issue in optimizing operational conditions is to examine the interactions of the variables and to find the optimal point where both adsorption capacity and reaction rate are maximal. RSM is one of the tools for studying the interactions between variables and simultaneously optimizing multiple responses [50].

So far, no optimal condition for sodium-based sorbent has been reported. In addition, the effects of the variables on the reaction kinetics have not yet been determined. In this work, RSM method using Box-Behnken Design (BBD) has been utilized to obtain the optimal values of the variables (temperature, vapor pretreatment time, and H_2O/CO_2 mole ratio). Initial CO_2 capture capacity (A_{ci}) and deactivation rate constant (k_d) were used as the responses for the optimization. Furthermore, BET, SEM, XRF, and XRD analyses were applied to compare the sorbent structure before and after the carbonation reaction.

EXPERIMENTAL SECTION

Sample Preparation

In this work, the sorbent (Na_2CO_3) is fixed on the support (γ-Al_2O_3) by applying the wet impregnation method [21]. Na_2CO_3 and γ-Al_2O_3 were supplied by Merck Company. The method consists of three steps: 1- The impregnation mixture is prepared. 2- It is dried at 100°C. 3- It is calcined at 300°C. Designated loading of Na_2CO_3 on the γ-Al_2O_3 was 35%, the actual amount loaded was 30% according to the XRF result. The Na_2CO_3/Al_2O_3 sorbent is denoted as NaAl where Al represents γ-Al_2O_3 and Na represents Na_2CO_3.

Sorbent Characterization

The actual loading amount of Na_2CO_3 was determined by a PHILIPS PW1480 X-Ray Fluorescence (XRF) system. The morphology of the sorbent was analyzed by Philips XL30 Scanning Electron Microscopy (SEM) system.

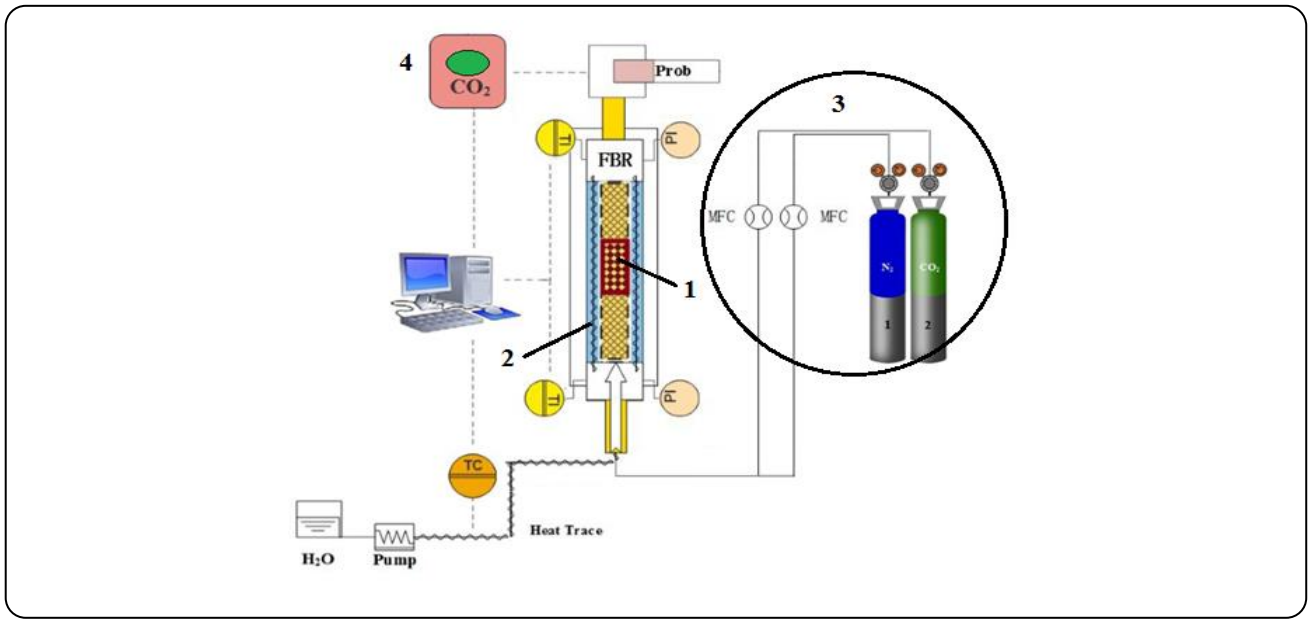

Fig. 1: Schematic diagram of the experimental apparatus for the fix-bed reactor.

The structural changes were analyzed by a PHILIPS PW 3830 X-Ray Diffraction (XRD) system. A PHS-1020 (PHSCHINA) system with N_2 adsorption-desorption was used to examine the specific surface area and pore volume.

Apparatus and Procedure

The carbonation reaction was performed in a Fixed Bed Reactor (FBR) as shown in Fig. 1. The experimental apparatus consists of four parts [46]. The first part is the fixed bed reactor, where the carbonation reaction occurs. The second section is a temperature bath consisting of two thermocouples in the inlet and outlet of the reactor to control the temperature. The third part is the gas injection system including gas cylinders and MFC, and the last section is CO_2 analyzer.

In each experiment, the amount of sorbent used in the bed was 3g, and the sorbent particle size was about 150-300 µm. In each cycle, the sorbent was regenerated at 300°C for 2 hours. The diameter of the reactor and the length of the reaction zone were 12 mm and 30 mm, respectively. The reactor temperature remained constant using the water flow in the FBR jacket, and this temperature could be controlled from 25°C to 90°C. The calibrated thermocouple determined the temperature of the bed at begin and end of the reactor. In all of the experiments, a steady flow of deionized water was heated to be evaporated entirely, and then the vapor was injected into the reactor. Heat tracing was used to hold the injection pipeline temperature sufficiently high to ensure that the vapor was not condensed before mixing with other gases. CO_2 and N_2 were provided from two separate cylinders with high purity and the Mass Flow Controllers (MFCs) were applied to regulate the gases flow rate. The total flow rate of the feed remained constant at 80 mL/min in all of the experiments. CO_2 concentration at the outlet of the bed was continuously measured by an online InfraRed (IR) analyzer (Vaisala, Finland, measurement limit 0−20 vol %).

In order to find the optimum point, a carbonation reaction occurred in different conditions. The experimental results at 40 ºC indicate that at low temperature causes vapor condensation, which can change the physical structure of the sorbent that in turn reduces the sorbent performance. Therefore, to ensure that the vapor condensation does not occur, the temperature of 50 °C is selected as the lowest temperature. In other words, 50 °C is the constraint of the optimization. Three different temperatures (50, 65, and 80°C) are applied to compare the effect of the adsorption temperature. For investigating the impact of H_2O/CO_2 mole ratio on carbonation reaction, the H_2O flow rate is constant in all of the experiments, and by changing the CO_2 flow rate, three mole ratios (0.5, 1, and 1.5) are obtained for H_2O/CO_2. The vapor pretreatment process to prepare sorbent is like injecting vapor into the bed for 3-9 minutes before the carbonation reaction is performed. The adsorption

Table 1: The volume concentrations of CO_2, H_2O, and N_2 for all experimental conditions.

Temperature	H_2O/CO_2 ratio	Vol (%) concentration		
		CO_2	H_2O	N_2
50	0.5	16.0	8.0	76
50	1	8 .0	8.0	84
50	1.5	5.4	5.4	89.2
65	0.5	16.1	8.1	75.8
65	1	8.5	8.5	83
65	1.5	5.6	5.6	88.8
80	0.5	17.7	8.8	73.5
80	1	8.9	8.9	82.2
80	1.5	5.9	5.9	88.2

operation is as follows: First, N_2 is injected into the bed for 1 hour to obtain the isothermal condition of the sorbent particles and to prevent the condensation of vapor at a low temperature. Second, the steady flow of the vapor is mixed with N_2 and injected into the bed for the vapor pretreatment process. In the end, after completion of the vapor pretreatment process, CO_2 is attached to the blend of the vapor and N_2, and then the adsorption operation is launched. Details for the volume concentrations are given in Table 1.

Analytical Basis

CO_2 capture capacity calculation

There are two different definitions of CO_2 capture capacity: Initial CO_2 capture capacity and total CO_2 capture capacity. Eq 1 can be used to calculate CO_2 capture capacity [46].

$$A_c = \frac{1000C_i}{w}\int_0^t Q\left(1-\psi(t)\right)\rho.dt \quad \left(\frac{mg_{CO_2}}{g_{sorbent}}\right) \tag{1}$$

Where A_c, w, C_i, Q, $\psi(t)$ and ρ are CO_2 capture capacity ($mgCO_2/g_{sorbent}$), sorbent mass (g), inlet CO_2 concentration (vol %), gas flow rate (cm^3/min), dimensionless outlet CO_2 concentration (C/C_i), and CO_2 density (g/cm^3), respectively. A_{ci} is the initial CO_2 capture capacity which is calculated by Eq 1 until the CO_2 concentration in the outlet gas is zero.

Deactivation Model

Generally, the activity of sorbent decreases with time as it is being used. Deactivation mechanism depends on the decay reactions, the presence or absence of pore diffusion, the way poisons act on the surface, etc. The variation of the activity over time which usually depends on the gas component concentration is calculated by Eq. (2) [51,52].

$$-\frac{da}{dt} = k_d C_i^{\,m} a^d \tag{2}$$

Where a is the activity of the sorbent, t is reaction time (min), k_d is deactivation rate constant (min^{-1}), C_i is the initial CO_2 concentration (vol %), d is named the order of deactivation, and m is the order of initial concentration.

Experimental Design

One of the most appropriate methods of experimental design is the RSM method. The advantages of this approach include analyzing the interactions between the variables, utilization of quadratic and cubic models for the analysis of the variables, and optimization of the multiple responses. Box-Behnken Design (BBD), due to the low number of experiments, is used to design the experiments with several variables. In BBD, all of the factors are investigated at three levels. In this work, RSM combined with BBD was used for the optimization of the operating conditions. Three factors; temperature, vapor pretreatment time, and H_2O/CO_2 mole ratio were selected as the variables, and the ranges of their variations are displayed in Table 2.

Table 2: Coded levels of the variables selected for BBD.

Independent variables	Unit	Symbol coded	Coded levels		
			-1	0	1
Temperature	°C	X_1	50	65	80
Vapor pretreatment Time	Min	X_2	3	6	9
H_2O/CO_2	-	X_3	0.5	1	1.5

Table 3: Textural properties of γ-Al2O3 and NaAl (before and after adsorption).

Sorbent	Surface area (m^2/g)	Pore volume (cm^3/g)	Mean pore size (nm)
γ–Al_2O_3	173.9	0.49	4.3
NaAl (fresh)	84.2	0.2	6.3
NaAl (used)	47.1	0.16	6.3

RSM suggested the quadratic model for examining the effect of the variables on both responses 'A_{ci}' and 'k_d'. The polynomial function with the quadratic term is shown in Eq. (3) [46].

$$Y = \beta_0 + \sum_{i=1}^{k} \beta_i X_i + \sum_{i=1}^{k} \beta_{ij} X_j^{\,2} + \sum_{1 \le i \le j}^{k} \beta_{ij} X_i X_j + \varepsilon \qquad (3)$$

Where Y is the predicted response, X_i and X_j are the variables, k is the number of the variables, β_0, β_i, β_{ii}, β_{ij} are regression coefficients for intercept, linear, quadratic, and interaction terms, respectively, and ε is the unanticipated error.

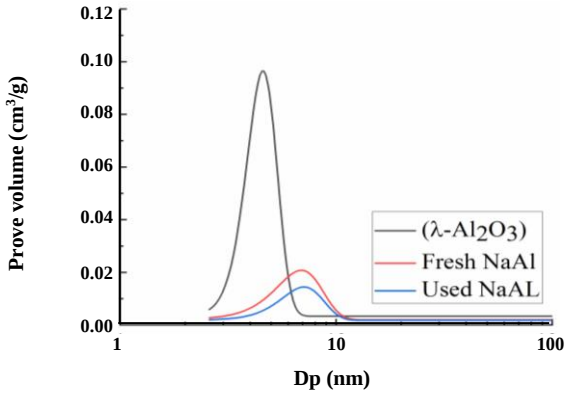

Fig. 2: PSD for γ-Al$_2$O$_3$ and NaAl (before and after adsorption).

RESULTS AND DISCUSSION

Characterization of sorbents

Porous structure performances

Some physical properties of a sorbent like the specific surface area have a significant influence on the adsorption process. Therefore, it is essential to deposit the sorbent on porous support [10]. N_2 adsorption-desorption analysis was employed to estimate the changes in the porous structure of the sorbent before and after the carbonation reaction. The pore volume and specific surface area of the pure alumina, the sorbent before adsorption (fresh), and the sorbent after adsorption (used) were calculated by Barrett–Joyner–Halenda (BJH) and Brunauer–Emmett–Teller (BET) methods, respectively. As it is seen in Table 3, the pore volume and the specific surface area of pure alumina are much higher than NaAl both before and after the carbonation reaction. The Pore Size Distribution (PSD) is shown in Fig. 2. γ-Al_2O_3 has a mesoporous structure (with pore diameter in the range of 2-50 nm). The peak point of γ-Al_2O_3 is 4.3 nm and after deposition of Na_2CO_3 on γ-Al_2O_3, the specific surface area, and pore volume are reduced, and the peak point is shifted toward the particles with a large pore diameter (6.3nm). These results may indicate that during the impregnation, first the smaller pores are filled. After the carbonation reaction, the peak point is not changed although both pore volume and specific surface area are reduced.

SEM Analysis

The distribution of Na_2CO_3 on the γ-Al_2O_3 before and after carbonation reaction is another important factor in this process. The morphology of the sorbent was determined by SEM analysis. SEM images with a magnification of 5000× were provided as displayed in Fig. 3. SEM images of fresh and used NaAl sorbents are shown in Fig. 3 that

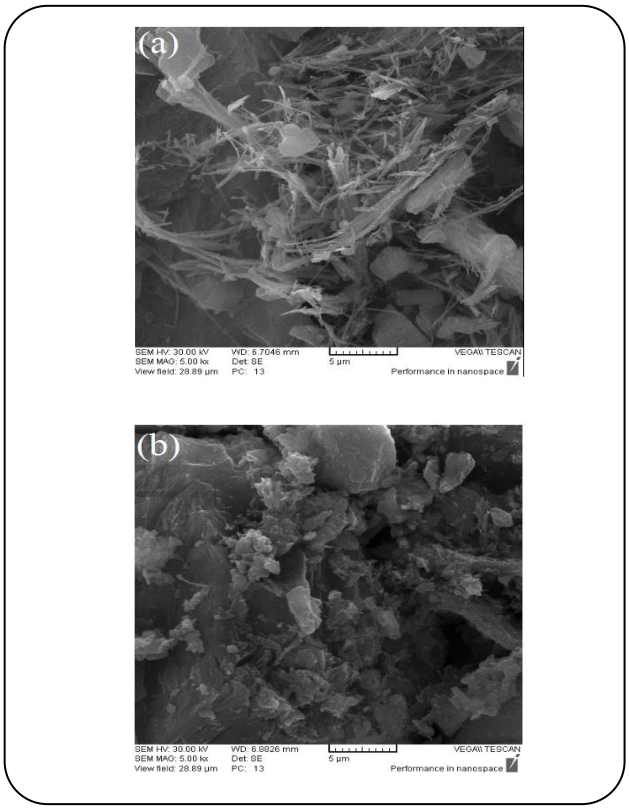

Fig. 3: SEM results of NaAl adsorbent: (a) before adsorption and (b) after adsorption in 16% CO_2 + 8% H_2O +76% N_2 at 50 °C.

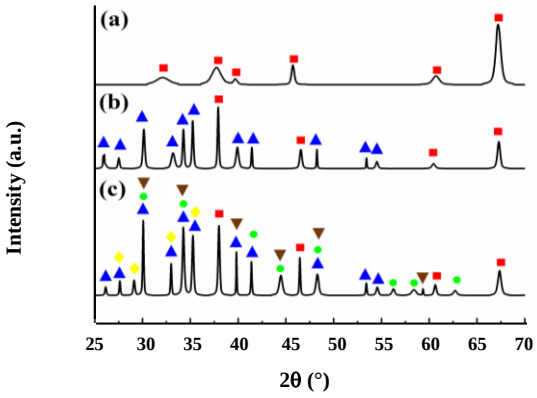

Fig. 4: XRD results for: (a) γ-Al_2O_3, (b) NaAl before adsorption, and (c) NaAl after adsorption in 16% CO_2 + 8% H_2O +76% N_2 at 50 °C: (■) γ-Al_2O_3, (▲) Na_2CO_3, (♦) Na_2CO_3*3$NaHCO_3$, (●) $NaHCO_3$, and (▼) Na_2CO_3*H_2O.

indicate the number of white fibers in Fig. 3a (fresh sorbent) is greater than Fig. 3b (used sorbent). SEM results, before the carbonation, reported by Zhao et al. also show that active components are distributed on the surface of γ-Al_2O_3 appearing like white fibers and spots [40].

XRD Analysis

The reaction products were evaluated by comparing the XRD pattern before and after carbonation reaction using X'Pert HighScore software. According to the X'Pert HighScore database, the cods for γ-Al_2O_3, Na_2CO_3, $NaHCO_3$, $Na_2CO_3.H_2O$, and $Na_2CO_3.3NaHCO_3$ are 00-048-0367, 00-001-1166, 00-002-0712, 00-002-0879, and 00-015-0653, respectively. XRD pattern of the support (γ-Al_2O_3) is shown in Fig. 4a. The sorbent pattern after loading Na_2CO_3 on the γ-Al_2O_3 is displayed in Fig. 4b that indicates the pattern only contains Na_2CO_3 and γ-Al_2O_3 peaks before the carbonation reaction. In order to obtain the XRD pattern, during the carbonation reaction, a fresh sorbent was placed under the reaction conditions (50 °C, with 9 minutes pretreatment time, and H_2O/CO_2=0.5) for 45 minutes. By analyzing the XRD pattern obtained in Fig. 4c, the reaction products can be identified. During the carbonation reaction, the phases formed from the carbonation reaction consists of $NaHCO_3$, $Na_2CO_3.H_2O$, and $Na_2CO_3.3NaHCO_3$ before the full saturation of the sorbent. As reported by *Luo et al.*, $NaHCO_3$ production was carried out from two pathways; either directly through reaction R2 or through reactions R3-R5 [49]. It has been reported that at temperatures above 70°C, only reaction R6 is occurred [16].

$$Na_2CO_3(s) + H_2O(g) = Na_2CO_3.H_2O(s) \quad \text{(R3)}$$

$$Na_2CO_3.H_2O(s) + 0.6CO_2(g) = 0.4(Na_2CO_3.3NaHCO_3)(s) + 0.4H_2O(g) \quad \text{(R4)}$$

$$0.4(Na_2CO_3.3NaHCO_3)(s) + 0.4CO_2(g) + 0.4H_2O(g) = 2NaHCO_3(s) \quad \text{(R5)}$$

$$Na_2CO_3(s) + 0.6H_2O(g) + 0.6CO_2(g) = 0.4(Na_2CO_3.3NaHCO_3)(s) \quad \text{(R6)}$$

CO_2 Breakthrough Curve of NaAl

According to our previous work, initial adsorption capacity is more important than the total adsorption capacity for the industry [50]. Therefore, the initial adsorption capacity was employed to optimize operating conditions. To calculate the kinetic parameters, the mass conservation equation of CO_2 in the fixed bed (Eq. (4)) with the supposition of the isothermal and pseudo-steady-state conditions are used.

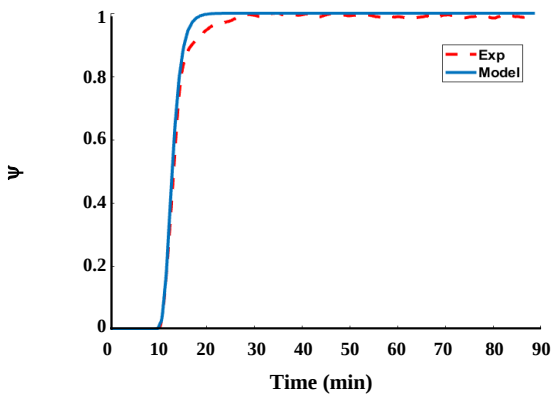

Fig. 5: Comparison of the experimental and modeling results (R^2 =0.99) with the BC (reaction conditions: 65 °C, with 6 min vapor pretreatment, and H_2O/CO_2=1).

$$\frac{d\psi}{dz} = -\frac{(1-\varepsilon_b)K}{\varepsilon_b \mu_g}\psi a$$

$$\psi = \frac{C}{C_i} \qquad (4)$$

Boundary condition: $z = 0 \Rightarrow \psi = 1$

Where Ψ, z, ε_b, μ_g, K, a, C, and C_i are dimensionless outlet CO_2 concentration (C/C_i), the total length of the bed (m), bed porosity, superficial velocity of gas flow (m/min), the reaction rate constant (min^{-1}), activity coefficient, outlet CO_2 concentration (vol %), and inlet CO_2 concentration (vol %). The CO_2 concentration profile was calculated by numerically solving Eq 2 (d=1 and m=0) and Eq 4 considering the initial and boundary conditions using the fourth-order Runge−Kutta method. Also, K and k_d were obtained using the nonlinear least-squares technique and the experimental data.

Fig. 5, shows a comparison of the breakthrough curve (BC) for the experimental and modeling results (under the reaction condition: 60 ºC, 6 min vapor pretreatment, and H_2O/CO_2 =1). As can be seen, the model's behavior is very similar to the experimental results and shows a high convergence (R^2= 99.6%). Therefore, using this model to calculate the kinetics of the reaction carbonation is sufficiently accurate. The kinetics factors for this experiment, K and k_d are equal to 210452.82 and 0.55 min^{-1}, respectively.

Analysis of variance (ANOVA)

A reliable method to assess the experimental data is the analysis of variance (ANOVA). In ANOVA, the scattering of the data is investigated by comparing the variances. The first response of the RSM applied in this research is the initial adsorption capacity (A_{ci}) and the second is the deactivation rate constant (k_d). The values of these responses at different experimental conditions are listed in Table 4.

ANOVA results for each response are shown in Table 5. The model can correctly predict the experimental data behavior if the P-value of the model and lack of fit are less than 0.05 and greater than 0.05, respectively. According to Table 5, the model P-values for both responses are smaller than 0.0001 which represents that the model is highly significant. Given that the P-value of lack of fit for both responses is higher than 0.05, so the effect of lack of fit on the model can be ignored.

The values of lambda for A_{ci} and k_d responses are considered to be 1 and 0, respectively. These values were suggested by analyzing the Box-Cox diagram (Fig. 6) with the RSM. The Box-Cox diagram is a tool to find the most appropriate transformation function for applying on the response. The minimum point of this graph shows the best value for lambda. In general, the use of the transfer function is suggested when the ratio of maximum to a minimum for a response is greater than 3. The ratio of maximum to a minimum for A_{ci} and k_d is 2.33 and 3.64, respectively. Therefore, the A_{ci} analysis does not require a transfer function, but it is recommended to use the natural logarithm function for k_d.

The effects of the parameters in the final response are presented in Table 6. By comparing the variables, it is clear that temperature has the most significant impact on 'A_{ci}'and 'k_d'. The second most effective parameter for A_{ci} is the vapor pretreatment time and for k_d is H_2O/CO_2 mole ratio. All of the variables have a significant effect on A_{ci}, but the impact of the vapor pretreatment time on k_d can be ignored against other variables.

Given the regression coefficients of the quadratic model in Table 6, Eq. (5) and Eq. (6) are estimated for modeling the effect of the variables on A_{ci} and k_d.

$$Y_1 = +30.66 - 8.84X_1 + 2.17X_2 - 1.63X_3 \qquad (7)$$
$$-1.65X_{12} + 1.32X_{13} - 1.64X_{23} - 2.29X_1^2 - 1.98X_2^2 - 1.89X_3^2$$

$$\ln(Y_2) = -0.61 + 0.34X_1 - 0.047X_2 - 0.29X_3 \qquad (8)$$
$$+0.029X_{12} - 0.008X_{13} + 0.027X_{23} +$$
$$0.11X_1^2 + 0.053X_2^2 + 0.082X_3^2$$

Table 4: RSM-BBD design matrix and experimental results for responses.

STD	Independent variables			Dependent variables	
	X_1	X_2	X_3	A_{ci} (mg CO_2/g sorbent)	k_d (min^{-1})
1	50	3	1	30.937	0.497
2	80	3	1	16.831	0.917
3	50	9	1	39.238	0.416
4	80	9	1	18.538	0.863
5	50	6	0.5	38.298	0.616
6	80	6	0.5	17.7	1.259
7	50	6	1.5	32.61	0.346
8	80	6	1.5	17.285	0.686
9	65	3	0.5	25.039	0.87
10	65	9	0.5	31.995	0.77
11	65	3	1.5	24.859	0.471
12	65	9	1.5	25.252	0.465
13	65	6	1	31.195	0.538
14	65	6	1	32.113	0.523
15	65	6	1	29.941	0.553
16	65	6	1	30.599	0.541
17	65	6	1	29.434	0.55

Table 5: Results of the ANOVA for the RSM-BBD model of responses.

	Analysis of variance A_{ci} (Lambda=1)					
Source	Sum of squares	Degree of freedom	Mean square	F-value	P-value	
Model	772.69	9	85.85	108.38	<0.0001	significant
Residual	5.54	7	0.79			
Lack of fit	1.12	3	0.37	0.34	0.799	not significant
Pure error	4.42	4	1.11			
Total	778.24	16				Total
	Analysis of variance k_d (Lambda=0)					
Source	Sum of squares	Degree of freedom	Mean square	F-value	P-value	
Model	1.73	9	0.19	317.79	<0.0001	significant
Residual	0.004	7	0.0006			
Lack of fit	0.002	3	0.0008	1.59	0.325	not significant
Pure error	0.002	4	0.0005			
Total	1.73	16				

Table 6: Results of the ANOVA for coefficients of the variables in the correlation of the responses.

	A_{ci}			k_d		
Coded parameters of the correlation	Estimated coefficient	F-value	P-value	Estimated coefficient	F-value	P-value
X_1	-8.84	789.42	<0.0001	0.34	1556.94	< 0.0001
X_2	2.17	47.54	0.0013	-0.047	28.90	0.0010
X_3	-1.63	26.78	0.0013	-0.29	1097.74	< 0.0001
X_1X_2	-1.65	13.72	0.0076	0.029	5.69	0.0485
X_1X_3	1.32	8.78	0.0210	-0.008	0.38	0.5558
X_2X_3	-1.64	13.59	0.0078	0.027	4.95	0.0615
X_1^2	-2.29	27.92	0.0011	0.11	83.43	< 0.0001
X_2^2	-1.98	20.81	0.0026	0.053	19.33	0.0032
X_3^2	-1.89	19.02	0.0033	0.082	47.02	0.0002

Table 7: The fitting indices of models obtained.

Analysis of variance (A_{ci})			
R^2	0.993	Std.Dev	0.89
R_{adj}^2	0.984	%C.V.	3.21
$R_{predict}^2$	0.968	PRESS	24.89
Analysis of variance (k_d)			
R^2	0.998	Std.Dev	0.025
R_{adj}^2	0.994	%C.V.	4.92
$R_{predict}^2$	0.977	PRESS	0.040

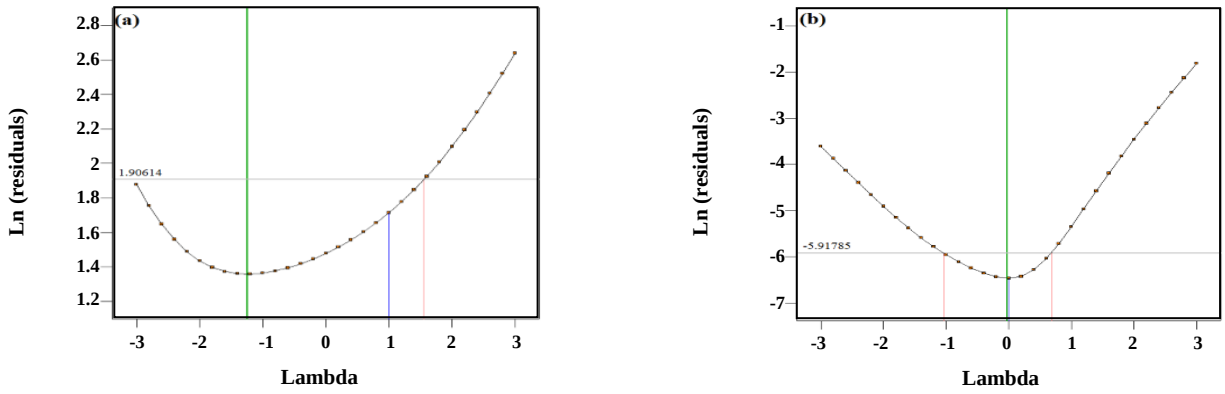

Fig. 6: Box-Cox diagram for power transform for (a) initial CO_2 capture capacity (A_{ci}) and (b) deactivation rate constant (k_d).

The fit indices of the models for each response are shown in Table 7. R-squared (R^2) indicates the degree of convergence of the experimental and model data. The values of R^2 are between 0 and 1, with 0 defining that model does not illustrate any variation and 1 explaining that it ultimately illustrates the observed variation. R^2_{adj} predicts the effects of the model coefficients which is more critical than R^2. $R^2_{predict}$ examines the model's ability to anticipate new observations. Besides, the values of Std. Dev, %C.V., and PRESS are listed in Table 7.

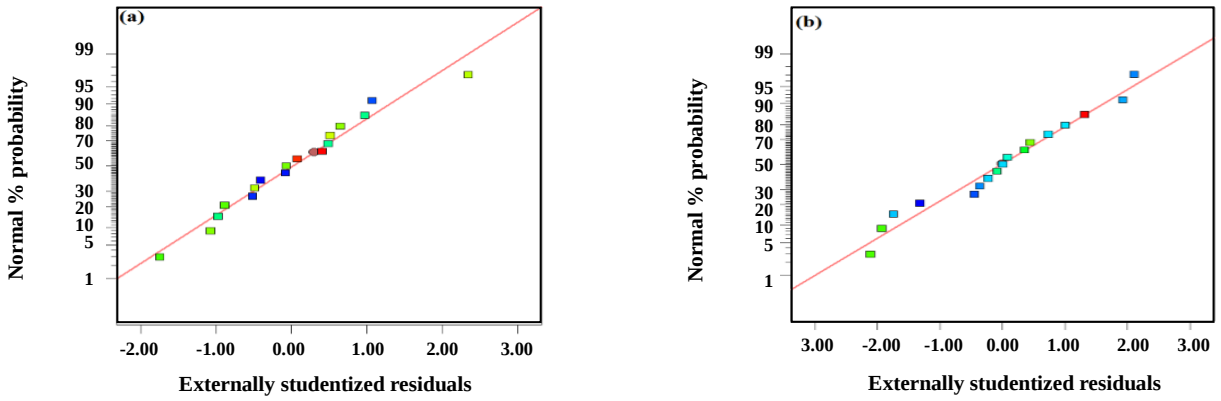

Fig. 7: The normal plot of the residuals for (a) initial CO_2 captures capacity (A_{ci}) and (b) deactivation rate constant (k_d).

The normal plot of the residuals is illustrated in Fig. 7. The residuals are described as the differences between the actual and the predicted values of the responses. In general, the normal probability diagram displays how the residuals follow a normal scattering. As it is clear, this chart is almost linear, so the distribution of the residuals is normal.

Effects of the Operating Conditions

To investigate the interactions between the variables and their effects on the final responses, the 3-D graphs of the surface response were applied. Figs. 8 and 9 show alterations of A_{ci} and k_d in terms of the variables. In these charts, one variable remains constant in the central point, and the response is expressed in terms of other variables.

Effect of Temperature

Since the carbonation reaction is exothermic, increasing temperature decreases the equilibrium constant and conversion of carbonation reaction according to Table 3. Therefore, adsorption capacity is sharply decreased at higher temperatures as shown in Fig. 8. Considering Table 6, the reaction temperature has the most significant impact on the responses. Consequently, in each molar ratio of H_2O/CO_2 and vapor pretreatment time, increasing temperature always decreases A_{ci} and enhances k_d. Thus, it is better to operate the process at the lowest temperature, although low operating temperature (around 40°C) in the fix bed reactor causes vapor condensation, which can change the physical structure of the sorbent and reduce the sorbent performance. Therefore, the lowest possible temperature to have the highest efficiency is accepted as 50 °C.

Effect of Vapor Pretreatment Time

As reported in the literature, the vapor pretreatment process can increase the adsorption capacity [39]. Therefore, vapor pretreatment time is used as a variable, and its effect on A_{ci} is displayed in Figs. 8a and 9a. According to section 3.1.3, CO_2 is adsorbed either directly through reaction R2 or reactions R3-R5, and $Na_2CO_3.H_2O$ is the primary reactant of reaction R4. During the vapor pretreatment, Na_2CO_3 is converted to $Na_2CO_3.H_2O$ through reaction R3, so the higher vapor pretreatment time prepares more $Na_2CO_3.H_2O$ and increases the amount of adsorbed CO_2. However, reaction R3 rarely takes place at temperatures above 70. Therefore, as shown in Fig. 8a and 8b, vapor pretreatment time does not have any effect on A_{ci} and k_d at high temperatures. Moreover, Figs. 8b and 9b show that the vapor pretreatment time has little impact on k_d.

Effect of H_2O/CO_2

To investigate the effects of H_2O/CO_2 mole ratio on the carbonation reaction, the H_2O flow rate was kept constant in all of the experiments while the mole ratio of H_2O/CO_2 was altered by changing the CO_2 flow rate. Thus, a reduction in CO_2 concentration caused an increase in H_2O/CO_2 mole ratio. The plots of k_d variations versus H_2O/CO_2 mole ratio are presented in Figs. 8d and 9b. Since the amount of the sorbent is constant during the adsorption process, reducing CO_2 concentration (increasing the H_2O/CO_2 mole ratio) causes enhancement of saturation time of sorbent and reduction of k_d. Fig. 8c and 9a indicate that a decrease in CO_2 concentration (an increase in H_2O/CO_2 mole ratio) has a negative impact on A_{ci} as it

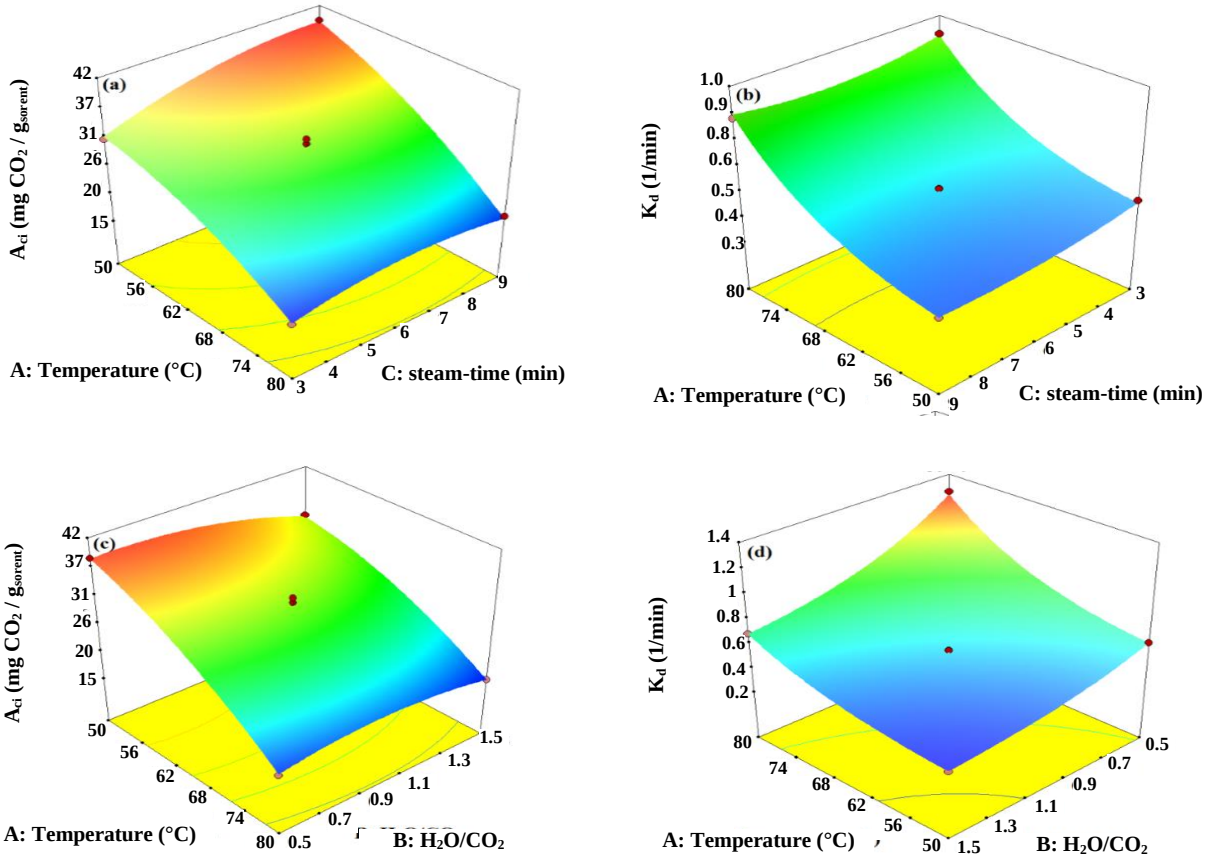

Fig. 8: 3D plots of initial CO_2 capture capacity (A_{ci}) and deactivation rate constant (k_d) as the functions of (a,b) temperature- vapor pretreatment time and (c,d) temperature- H_2O/CO_2, plots were supplied as the functions of two variables at the middle amounts of the other variables.

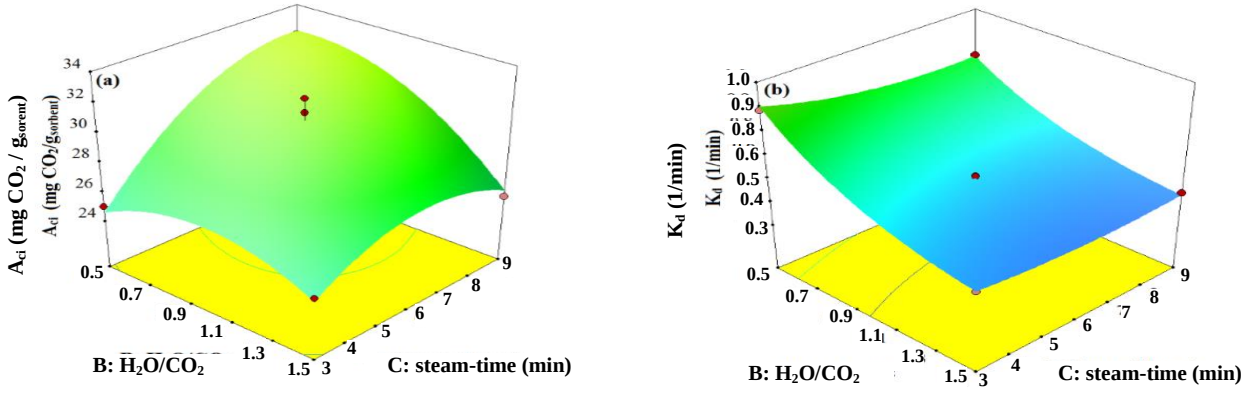

Fig. 9: 3D plots of (a) initial CO_2 capture capacity (A_{ci}) and (b) deactivation rate constant (k_d) as the function of H_2O/CO_2- vapor pretreatment time, plots were supplied as the functions of two variables at the average amounts of the other variable.

causes a lower concentration of the gas component reactant of reactions R2, R4, and R5, so the rates of these reactions are decreased. It can be concluded that by increasing CO_2 (reducing H_2O/CO_2 mole ratio) more amount of CO_2 is adsorbed in a shorter time, which means higher A_{ci} and k_d.

The effect of H_2O/CO_2 mole ratio is mainly dependent on the rate of carbonation reactions. Moreover, as mentioned in section 3.1.3, at a temperature above 70 only reaction R6 occurs. Therefore, the effect of the H_2O/CO_2 mole ratio is reduced at high temperatures as indicated

Table 8: Optimization results of the independent variables

Process variables	Optimal value
Temperature (^{o}c)	50
Vapor pretreatment time (min)	9
H_2O/CO_2	1

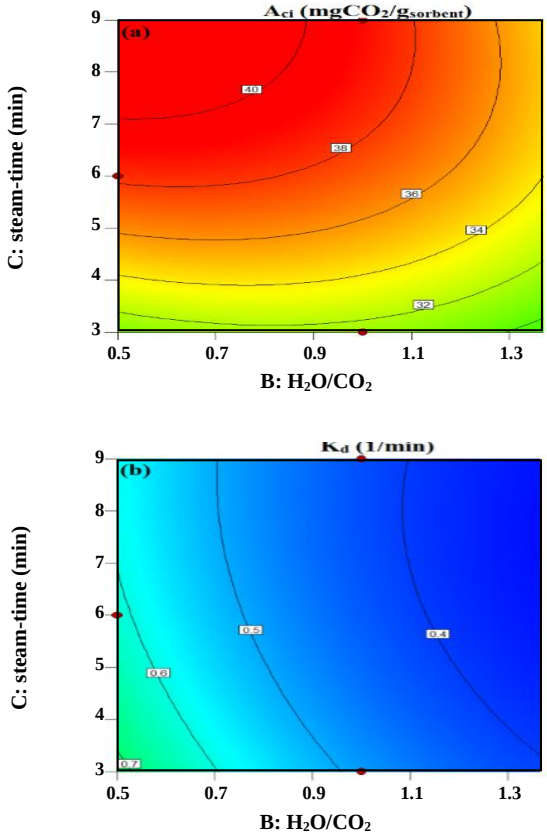

Fig. 10: 2D Contour plots of (a) initial CO_2 capture capacity (A_{ci}) and (b) deactivation rate constant (k_d) at 50 °C as functions of H_2O/CO_2 and vapor pretreatment time.

by the results of Fig. 8c and 8d. Figs. 9a and 9b show that the effect of vapor pretreatment time is decreased at a low H_2O/CO_2 mole ratio. Since CO_2 does not contribute to reaction R3, the formation of $Na_2CO_3.H_2O$ through vapor pretreatment can only increase the amount of CO_2 adsorption if the condition is suitable for reactions R4 and R5 to occur. In addition, as mentioned above, reducing CO_2 concentration leads to a higher H_2O/CO_2 mole ratio and a lower concentration of the gas component reactant. As a result, it reduces the rates of the reactions R4 and R5, so weakening the effect of vapor pretreatment time.

Optimization of Operating Conditions

A_{ci} and k_d were simultaneously optimized using RSM. The optimal values of the parameters were found at the point where A_{ci} is maximized and k_d is minimized. The optimal operating conditions are displayed in Table 8.

Table 8 indicates that 50 °C is the optimal temperature, which also does not cause vapor condensation as explained in section 2.3. That means high efficiency at low temperature can be achieved using this sorbent which is one of the best advantages of sodium-based-sorbents. The optimal amounts for the vapor pretreatment time and H_2O/CO_2 mole ratio were reported to be equal to 9 minutes and 1, respectively. The diagram of the contour plots for the optimum point at constant temperature (T=50 °C) is shown in Fig. 10. The optimal values for A_{ci} and k_d were calculated to be 39.298 $mgCO_2/g_{sorbent}$ and 0.416 min^{-1}, respectively.

In Table 9, the experimental results are compared with the predicted values of the RSM model in the optimal operating conditions. As it is obvious, the experimental results and the predicted values are very close to each other.

CONCLUSIONS

The goals of this work were to investigate the effects of the operating conditions on the CO_2 capture process using Na_2CO_3-based sorbent in a fixed bed reactor as well as finding the optimal operating conditions applying the RSM method. Temperature, vapor pretreatment time, and H_2O/CO_2 mole ratio were considered as the influencing variables and A_{ci} and k_d as the responses to design the experiments. A_{ci} was calculated using the breakthrough curve as the CO_2 concentration in the output gas was zero. k_d was calculated by simultaneously solving the deactivation model and the mass conservation in the fix bed reactor using the experimental data and nonlinear-least-square technique. In addition, the quadratic polynomial function was used for modeling and optimization. The variations in the sorbent structure, before and after the carbonation reaction, were evaluated by SEM and BET analyses. The SEM images indicated that the physical structure of the sorbent was changed during the carbonation reaction. The BET results showed both pore volume and specific surface area of the sorbent were reduced after the carbonation reaction. The pattern obtained by XRD analysis confirmed the formation of $NaHCO_3$, $Na_2CO_3.H_2O$, and $Na_2CO_3.{}_3NaHCO_3$ as the reaction products.

Table 9: Predicted and experimental responses values at optimum conditions.

Dependent variables	Actual value	Predicted value	Error (%)
A_{ci} (mg $CO_2/g_{sorbent}$)	39.238	39.05	0.48
k_d (min^{-1})	0.416	0.423	1.7

The ANOVA results indicated that the model could adequately predict the experimental data. Moreover, the results revealed that among the parameters, the temperature has the most significant impact on the responses. The experimental results showed that since reactions R2-R6 are exothermic, temperature reduction improved the adsorption process. In the case of interactions between the variables, it was revealed that the effects of H_2O/CO_2 mole ratio and vapor pretreatment time at the high temperatures were reduced. Furthermore, increasing H_2O/CO_2 mole ratio decreased the impact of vapor pretreatment time. The optimum conditions were obtained at a temperature of 50 ºC, vapor pretreatment time of 9 min, and H_2O/CO_2 mole ratio of 1. The values of A_{ci} and k_d at the optimal point were calculated as 39.298 $mgCO_2/g_{sorbent}$ and 0.416 min^{-1}, respectively.

Nomencluture

A_{ci}	Initial CO_2 capture capacity
a	Sorbent activity
C	Outlet CO_2 concentration, vol %
C_i	Inlet CO_2 concentration, vol %
d	The order of deactivation
K	Reaction rate constant, min^{-1}
K_{eq}	Equilibrium constant
k_d	Deactivation rate constant, min^{-1}
M_{CO2}	Molecular weight of CO_2, g/mol
m	The order of initial concentration
Q	Gas flow rate, cm^3/min
R	Gas constant, kJ/mol·K
t	Reaction time, min
T	Temperature, K
u_g	Superficial velocity of gas flow, m/min
X	Independent variable
Y	Predicted response
w	Sorbent mass, g
z	Axial coordinate in a fixed bed, m
β	Regression coefficient
ΔG^0	Standard Gibbs free energy change, kJ/mol
ΔH^0	Standard enthalpy change, kJ/mol
ΔS^0	Standard entropy change, kJ/K
ε	Unanticipated error
ε_b	Bed porosity
ζ	Dimensionless length of bed
ρ	CO_2 density, g/cm^3
τ	Time scale of flow through the bed, min
ψ	Dimensionless outlet CO_2 concentration, C/C_i
0	Intercept term
i	Linear term
ii	Quadratic term
ij	Interaction term

Abbreviations

A_{ci}	Initial CO_2 capture capacity
A_{ct}	Total CO_2 capture capacity
ANOVA	Analysis of variance
BBD	Box–Behnken design
BC	Breakthrough curve
BET	Brunauer-Emmett-Teller
BJH	Barrett-Joyner-Halenda
FBR	Fixed bed reactor
IR	InfraRed
NaAL	Na_2CO_3/Al_2O_3
PSD	Pore Size Distribution
RSM	Response surface methodology
SEM	Scanning electron microscopy
XRD	X-Ray Diffraction
XRF	X-Ray Fluorescence

Received : May 4, 2020 ; Accepted : Jul. 20, 2020

REFERENCES

[1] Moussa M., Bader N., Querejeta N., Durán I., Pevida C., Ouederni A., Toward Sustainable Hydrogen Storage and Carbon Dioxide Capture in Post-combustion Conditions, *J. Environ. Chem. Eng.*, **5(2)**:1628–37 (2017).

[2] Lee S-Y., Park S-J., A Review on Solid Adsorbents for Carbon Dioxide Capture, *J. Ind. Eng. Chem.*, **23**: 1–11 (2015).

[3] Akhter P., Farkhondehfal M.A., Hernández S., Hussain M., Fina A., Saracco G., Khan A.U., Russoet N., Environmental Issues Regarding CO_2 and Recent Strategies for Alternative Fuels Through Photocatalytic Reduction with Titania-Based Materials, *J. Environ. Chem. Eng.*, **4(4)**: 3934–3953 (2016).

[4] van den Broek M., Hoefnagels R., Rubin E., Turkenburg W., Faaij A., Effects of Technological Learning on Future Cost and Performance of Power Plants with CO_2 Capture, *Prog. Energy Combust. Sci*, **35(6)**: 457–80 (2009).

[5] Mukherjee S., Kumar P., Yang A., Fennell P., Energy and Exergy Analysis of Chemical Looping Combustion Technology and Comparison with Pre-combustion and Oxy-Fuel Combustion Technologies for CO_2 Capture, *J. Environ. Chem. Eng.*, **3(3)**: 2104–14 (2015).

[6] Qin C., Yin J., Ran J., Zhang L., Feng B., Effect of Support Material on the Performance of K_2CO_3-Based Pellets for Cyclic CO_2 Capture, *Appl Energy*, **136**:280–8 (2014).

[7] Song C., Global Challenges and Strategies for Control, Conversion and Utilization of CO_2 for Sustainable Development Involving Energy, Catalysis, Adsorption and Chemical Processing, *Catal Today*, **115(1)**: 2–32 (2006).

[8] Cutting R.H., Cahoon L.B., Hall J.C., If the Tide is Rising, Who Pays for the Ark? *Coast Manag.*, **39(3)**: 282–295 (2011).

[9] Chang F., Zhou J., Chen P., Chen Y., Jia H., Saad S.M.I., Gao Y., Cao X., Zheng T., Microporous and Mesoporous Materials for Gas Storage and Separation: A Review, *Asia-Pacific J. Chem. Eng.*, **8(4)**: 618–626 (2013).

[10] Zhao C., Chen X., Anthony E.J., Jiang X., Duan L., Wu Y., Dong W., Zhao C., Capturing CO_2 in Flue Gas from Fossil Fuel-Fired Power Plants Using Dry Regenerable Alkali Metal-Based Sorbent, *Prog. Energy Combust. Sci.*, **39(6)**: 515–534 (2013).

[11] Anderson C., Ho M., Harkin T., Wiley D., Hooper B., Large Scale Economics of a Precipitating Potassium Carbonate CO_2 Capture Process for Black Coal Power Generation, *Greenh Gases Sci. Technol.*, **4(1)**:8–19 (2014).

[12] Ko J-J., Li M-H., Kinetics of Absorption of Carbon Dioxide into Solutions of N-methyldiethanolamine+ Water, *Chem. Eng. Sci.*, **55(19)**: 4139–4147 (2000).

[13] Ashraf Talesh S.S., Fatemi S., Hashemi S.J., Emrani P., Comparative Study of Carbon Dioxide and Methane Adsorption by Synthesized Fine Particles of SAPO-34 Molecular Sieve, *Iran. J. Chem. Chem. Eng. (IJCCE)*, **29(3)** 37–45 (2010).

[14] Nazari Kudahi S., Noorpoor A.R., Mahmoodi N.M., Adsorption Performance Indicator for Power Plant CO_2 Capture on Graphene Oxide/TiO_2 Nanocomposite, *Iran. J. Chem. Chem. Eng. (IJCCE)*, **38(3)**:293–307 (2019).

[15] Samanta A., Zhao A., Shimizu G.K.H., Sarkar P., Gupta R., Post-Combustion CO_2 Capture Using Solid Sorbents: A Review, *Ind. Eng. Chem. Res.*, **51(4)**:1438–63 (2011).

[16] Liang Y., Harrison D.P., Gupta R.P., Green D.A., McMichael W.J., Carbon Dioxide Capture Using Dry Sodium-Based Sorbents, *Energy & Fuels*, **18(2)**:569–75 (2004).

[17] Li L., Zhao N., Wei W., Sun Y., A Review of Research Progress on CO_2 Capture, Storage, and Utilization in Chinese Academy of Sciences, *Fuel*, **108**:112–30 (2013).

[18] Lee J.B., Ryu C.K., Baek J-I., Lee J.H., Eom T.H., Kim S.H., Sodium-Based Dry Regenerable Sorbent for Carbon Dioxide Capture from Power Plant Flue Gas, *Ind. Eng. Chem. Res.*, **47(13)**:4465–72 (2008).

[19] Veselovskaya J.V., Derevschikov V.S., Kardash T.Y., Stonkus O.A., Trubitsina T.A., Okunev A.G., Direct CO_2 Capture from Ambient Air Using K_2CO_3/Al_2O_3 Composite Sorbent, *Int. J. Greenh. Gas. Control.*, **17**:332–40 (2013).

[20] Dong W., Chen X., Yu F., Wu Y., $Na_2CO_3/MgO/Al_2O_3$ Solid Sorbents for Low-Temperature CO_2 Capture, *Energy & Fuels*, **29(2)**: 968–973 (2015).

[21] Kondakindi R.R., McCumber G., Aleksic S., Whittenberger W., Abraham M.A., Na_2CO_3-Based Sorbents Coated on Metal Foil: CO_2 Capture Performance, *Int. J. Greenh. Gas Control.*, **15**:65–9 (2013).

[22] Jaiboon O., Chalermsinsuwan B., Mekasut L., Piumsomboon P., Effect of Flow Patterns/Regimes on CO_2 Capture Using K_2CO_3 Solid Sorbent in Fluidized Bed/Circulating Fluidized Bed, *Chem. Eng. J.*, **219**:262–72 (2013).

[23] Dong W., Chen X., Wu Y., Zhao C., Liang C., Liu D., Carbonation Characteristics of Dry Sodium-Based Sorbents for CO_2 Capture, *Energy & Fuels*, **26(9)**:6040–6 (2012).

[24] Olajire AA., Synthesis of Bare and Functionalized Porous Adsorbent Materials for CO_2 Capture, *Greenh. Gases Sci. Technol.*, **7(3)**:399–459 (2017).

[25] Okunev A.G., Sharonov V.E., Gubar A.V., Danilova I.G., Paukshtis E.A., Moroz E.M., Kriger T.A., Malakhov V.V., Aristov Yu.I., Sorption of Carbon Dioxide by the Composite Sorbent 'Potassium Carbonate in Porous Matrix', *Russ. Chem. Bull*. **52(2)**:359–63 (2003).

[26] Zhao C., Chen X., Zhao C., CO_2 Absorption Using Dry Potassium-Based Sorbents With Different Supports, *Energy & Fuels*, **23(9)**:4683–4687 (2009).

[27] Okunev A.G., Sharonov V.E., Aristov Y.I., Parmon V.N., Sorption of Carbon Dioxide from Wet Gases by K_2CO_3-in-Porous Matrix: Influence of the Matrix Nature, *React. Kinet. Catal. Lett.*, **71(2)**:3 55–62 (2000).

[28] Dutcher B., Fan M., Leonard B., Dyar M.D., Tang J., Speicher E.A., Liu P., Zhang Y., Use of Nanoporous FeOOH as a Catalytic Support for $NaHCO_3$ Decomposition Aimed at Reduction of Energy Requirement of $Na_2CO_3/NaHCO_3$ Based CO_2 Separation Technology, *J. Phys. Chem. C*, **115(31)**:15532–44 (2011).

[29] Tuwati A., Fan M., Russell A.G., Wang J., Dacosta H.F.M., New CO_2 Sorbent Synthesized with Nanoporous $TiO(OH)_2$ and K_2CO_3, *Energy & Fuels*, **27(12)**:7628–36 (2013).

[30] Lee S.C., Choi B.Y., Lee S.J., Jung S.Y., Ryu C.K., Kim J.C., CO_2 Absorption and Regeneration Using Na and K Based Sorbents, *Stud Surf Sci Catal*, **153**:527–30 (2004).

[31] Dutcher B., Fan M., Leonard B., Use of Multifunctional Nanoporous $TiO(OH)_2$ for Catalytic $NaHCO_3$ Decomposition-Eventually for $Na_2CO_3/NaHCO_3$ Based CO_2 Separation Technology, *Sep. Purif. Technol.*, **80(2)**: 364–74 (2011).

[32] Cho M.S., Lee S.C., Chae H.J., Lee J.B., Kim J.C., Preparation and Performance of Potassium-Based Sorbent Using SnO_2 for Post-Combustion CO_2 Capture, *Adsorption*, **22(8)**:1119–27 (2016).

[33] Zhang B-T., Fan M., Bland A.E., CO_2 Separation by a New Solid K−Fe Sorbent, *Energy & Fuels*, **25(4)**:1919–25 (2011).

[34] Lee S.C., Choi B.Y., Lee T.J., Ryu C.K., Ahn Y.S., Kim J.C., CO_2 Absorption and Regeneration of Alkali Metal-Based Solid Sorbents, *Catal. Today*, **111(3)**: 385–390 (2006).

[35] Saadatjou N., Jafari A., Sahebdelfar S., Synthesis and Characterization of Ru/Al_2O_3 Nanocatalyst for Ammonia Synthesis, *Iran. J. Chem. Chem. Eng. (IJCCE)*, **34**(1):1–9 (2015).

[36] Kazemi H., Shahhosseini S., Bazyari A., Amiri M., A Study on the Effects of Textural Properties of γ-Al_2O_3 Support on CO_2 Capture Capacity of Na_2CO_3, *Process Saf. Environ. Prot*, **138**:176–185 (2020).

[37] Sengupta S., Amte V., Dongara R., Das A.K., Bhunia H., Bajpai P.K., Effects of the Adsorbent Preparation Method for CO_2 Capture from Flue Gas Using K_2CO_3/Al_2O_3 Adsorbents, *Energy & Fuels*, **29(1)**:287–297 (2014).

[38] Dinda S., Development of Solid Adsorbent for Carbon Dioxide Capture from Flue Gas, *Sep. Purif. Technol.*, **109**:64–71 (2013).

[39] Seo Y., Jo S-H., Ryu C.K., Yi C-K., Effects of Water Vapor Pretreatment Time and Reaction Temperature on CO_2 Capture Characteristics of a Sodium-Based Solid Sorbent in a Bubbling Fluidized-Bed Reactor, *Chemosphere*, **69(5)**:712–718 (2007).

[40] Zhao C., Chen X., Zhao C., Wu Y., Dong W., K_2CO_3/Al_2O_3 for Capturing CO_2 in Flue Gas from Power Plants. Part 3: CO_2 Capture Behaviors of K_2CO_3/Al_2O_3 in a Bubbling Fluidized-bed Reactor, *Energy & Fuels*, **26(5)**:3062–3068 (2012).

[41] Yi C-K., Jo S-H., Seo Y., Lee J-B., Ryu C-K., Continuous Operation of the Potassium-Based Dry Sorbent CO_2 Capture Process with Two Fluidized-Bed Reactors, *Int. J. Greenh Gas Control*, **1(1)**: 31–36 (2007).

[42] Zhao C., Chen X., Zhao C., Study on CO_2 Capture Using Dry Potassium-Based Sorbents Through Orthogonal Test Method, *Int. J. Greenh. Gas Control*, **4**(4):655–8 (2010).

[43] Zhao C., Guo Y., Li C., Lu S., Carbonation Behavior of K_2CO_3/AC in Low Reaction Temperature and CO_2 Concentration, *Chem. Eng. J.*, **254**:524–30 (2014).

[44] Lee S.C., Choi B.Y., Ryu C.K., Ahn Y.S., Lee T.J., Kim J.C., The Effect of Water on the Activation and the CO_2 Capture Capacities of Alkali Metal-Based Sorbents, *Korean J Chem Eng*, **23(3)**:374–379 (2006).

[45] Yu F., Wu Y., Zhang W., Cai T., Xu Y., Chen X., A Novel Aerogel Sodium-Based Sorbent for Low Temperature CO_2 Capture, *Greenh Gases Sci Technol*, **6(4)**:561–73 (2016).

[46] Rodríguez-Mosqueda R., Bramer E.A., Brem G., CO_2 Capture from Ambient Air Using Hydrated Na_2CO_3 Supported on Activated Carbon Honeycombs with Application to CO_2 Enrichment in Greenhouses, *Chem. Eng. Sci.*, **189(2)**:114-122 (2018).

[47] Wu Y., Chen X., Zhao C., Study on the Failure Mechanism of Potassium-Based Sorbent for CO_2 Capture and the Improving Measure, *Int. J. Greenh. Gas. Control.*, **5**(5):1184–9 (2011).

[48] Shi X., Xiao H., Lackner K.S., Chen X., Capture CO_2 from Ambient Air Using Nanoconfined Ion Hydration, *Angew. Chemie.*, **128(12)**:4094–4097 (2016).

[49] Luo H., Kanoh H., Fundamentals in CO_2 Capture of Na_2CO_3 Under a Moist Condition, *J. Energy Chem.*, **26(5)**:972–983 (2017).

[50] Amiri M., Shahhosseini S., Ghaemi A., Optimization of CO_2 Capture Process from Simulated Flue Gas by Dry Regenerable Alkali Metal Carbonate Based Adsorbent Using Response Surface Methodology, *Energy & Fuels*, **31(5)**:5286–5296 (2017).

[51] Jongartklang N., Chanchairoek S., Piumsomboon P., Chalermsinsuwan B., Correlations of Kinetic Parameters With Various System Operating Conditions for CO_2 Sorption Using K_2CO_3/Al_2O_3 Solid Sorbent in a Fixed/Fluidized Bed Reactor, *J. Environ. Chem. Eng,*. **4(2)**:1938–1947 (2016).

[52] Levenspiel O., Chemical Reaction Engineering, *Ind. Eng. Chem. Re.s*, **38(11)**:4140–4143 (1999).